PRODUCTION, TRANSPORT, AND DESTRUCTION OF DUST IN THE KUIPER BELT: THE EFFECTS OF REFRACTORY AND VOLATILE GRAIN COMPOSITIONS

THOMAS CORBETT

Department of Physics

University of Colorado at Boulder

March 17, 2025

Thesis Advisor: Prof. Mihály Horányi, Department of Physics

Honors Council Representative: Prof. Tobin Munsat, Department of Physics

Outside Reader: Prof. Zoltan Sternovsky, Aerospace Engineering

Abstract

The Venetia Burney Student Dust Counter (SDC) onboard the New Horizons spacecraft measures the spatial and size distributions of dust along its trajectory. Models based on early SDC measurements predicted a peak dust number density at a heliocentric distance of $\sim$40 au, followed by a rapid decline. Instead, SDC observed dust fluxes 2–3 times higher than predicted between 40 and 60 au. One potential explanation for this discrepancy is that SDC may be encountering icy grains with different dynamical behavior than previously modeled silicate grains. Due to ultraviolet photo-sputtering, water-ice grains rapidly erode and migrate outward, significantly contributing to the measured dust number densities only at distances $\gtrsim$40 au. We present a model of silicate and ice grain dynamics in the outer Solar System, considering gravitational and radiation forces and grain erosion. Using SDC data, we estimate that the mass production rate of ice grains between 0.1 and 10 μm in the Kuiper Belt (KB) would need to be 20–70 times higher than that of silicate grains. However, KB grains are expected to be refractory/volatile mixtures rather than pure silicate or ice. Thus, we briefly explore simple models of more realistic mixed-grain cases to further gauge the effects of grain composition on the equilibrium dust distribution. Future SDC measurements at greater distances will test the model predictions and further constrain silicate and ice grain production rates in the KB.

Acknowledgements

I thank my advisor, Dr. Mihály Horányi, PhD student Alex Doner, and the New Horizons team for their guidance, feedback, and patience. I also acknowledge the New Horizons team and the Charles A. Barth Scholarship for Undergraduate Space Research for their financial support. Finally, I am deeply grateful for the love and support of my parents throughout my academic journey.

Contents

1 Introduction **1**

2 The Student Dust Counter **2**

3 Source Objects **5**

4 Grain Dynamics **6**

5 Dust Production **10**

6 Results **12**

7 Discussion **14**

8 Conclusion **16**

List of Tables

1 Mass production rates of 0.1 to 10 μm silicate and ice grains for various KBO databases/models fitted to SDC data in the 1σ significance level. 14

List of Figures

1 **Left:** New Horizons flight path through 55 au in the J2000 reference frame. SDC minimum detectable mass is indicated by the color scale and increasing as New Horizons is slowing down due to the gravity of the Sun. The giant planets Jupiter, Saturn, Uranus, and Neptune, along with KBOs Pluto and Arrokoth, and the ISD inflow are shown. **Right:** All non-coincident SDC data above the minimum mass threshold as both measured impact charge and calculated grain mass with the corresponding radius indicated by the color scale through July 25th, 2023. The shaded regions indicate periods of high spacecraft activity during close encounters with Pluto and Arrokoth. Figure adapted from Doner et al., 2024. 3

2 SDC density measurements above 4 cutoff sizes: 0.63 μm, 0.68 μm, 0.82 μm, and 1.50 μm. The 0.63 μm, 0.82 μm, and 1.50 μm cutoff sizes are chosen based on instrument thresholds, whereas the 0.68 μm cutoff size is chosen to avoid any contribution from ISDs. Figure adapted from Doner et al., 2024. . 4

3 KBO orbital elements for the SBDB (green), CFEPS (blue), and OSSOS (red) databases/models. **Top:** eccentricity, e, as a function of semi-major axis, a. **Bottom:** inclination i as a function of semi-major axis, a. 6

4 Normalized distributions of KBO orbital elements. From top to bottom: the semi-major axis, eccentricity, and inclination of the SBDB (green), CFEPS (blue), and OSSOS (red) distributions. 7

5 Radiation pressure parameter β for silicate (red) and ice (blue) grains as a function of grain radius s (Burns, Lamy, and Soter, 1979). SDC mass thresholds for both silicate and ice grains are shown as crosses with the respective color. 8

6 Numerically integrated orbital evolution of initially 1 μm radius silicate (red) and ice (blue) grains from a source object on a circular orbit at 40 au, inclined by 5°. **Top:** Evolution of the semi-major axis (solid) and perihelion distance (dashed). These orbital elements are calculated with $\mu^* = \mu(1 - \beta)$ and represent the grain's orbital geometry. **Bottom:** Evolution of radiation pressure parameter (solid) and the ratio of grain size to initial grain size (dashed). . . 9

7 Keplerian orbits for example objects with semi-major axes $a = 30$ au and eccentricities $e = 0.0$ (blue), $e = 0.4$ (green), and $e = 0.8$ (red). The crosses indicate the positions of the objects at evenly spaced time intervals, determined by solving Kepler's equation for uniformly distributed mean anomalies. 11

8 Normalized probability density $n(s)$ as a function of initial grain radius s. . . 11

9 **Left:** Equilibrium number density profiles of silicate and ice grains near the ecliptic and above the SDC mass threshold as a function of heliocentric distance using the SBDB (top), CFEPS (middle) and OSSOS (bottom) KBO databases/models. The combined modeled number density (black) of silicate (red) and ice (blue) grains is fitted to SDC data with 1σ error bars (black) for heliocentric distances greater than 10 au. **Right:** Corresponding χ^2 maps of silicate and ice mass production rates for each KBO database/model with best-fit production rates (white crosses). Regions of confidence corresponding to a significance level of $\alpha = 0.68$ and $\alpha = 0.99$, or 1σ and 3σ, respectively, are encircled in white lines. 1σ production rate ranges can be found in Table 1. 13

10 Equilibrium number density profiles of well-mixed (top) and differentiated (bottom) grains near the ecliptic and above the SDC mass threshold as a function of heliocentric distance using the SBDB KBO database. Each histogram is labeled with its corresponding ice mass fraction. The same number of grains is produced for each case, matching the best-fit silicate production rate for the SBDB KBO database in Table 1. 15

1 Introduction

Interplanetary dust grains play a role in many physical processes such as the formation and evolution of planetary bodies, rings, and dusty exospheres (Thiessenhusen et al., 2002), as well as the transport of material into the magnetospheres and atmospheres of planetary bodies (Christon et al., 2015; Moses, 1992). The dust environment in the inner Solar System has been extensively researched through computational modeling, in-situ measurement, and remote sensing (e.g. Andrew R. Poppe, 2016; M. Horányi et al., 2008; Hillier et al., 2007), yet the dust environment of the outer Solar System is less understood.

The Venetia Burney Student Dust Counter (SDC) onboard the New Horizons spacecraft is the first dedicated dust instrument to make in-situ measurements beyond a heliocentric distance of 18 au. Measurements from SDC have been used to estimate the Kuiper Belt (KB) grain production rate and initial ejecta size distribution from the measured spatial and size distributions throughout the Solar System (Han et al., 2011; Andrew R. Poppe, 2016; A. R. Poppe et al., 2019). Based on SDC data from 5–40 au, early models predicted a peak number density of $\sim$30 km^{-3} for grains above the SDC mass threshold ($m \geq 2.62 \times 10^{-12}$ g) at a distance of $\sim$40 au. The number density was also predicted to decrease by a factor of $\sim$2 by 50 au with a continued decline at greater distances (Andrew R. Poppe, 2016; A. R. Poppe et al., 2019). Contrary to expectations, however, SDC reported roughly constant fluxes between 40 and 60 au (Doner et al., 2024).

Possible explanations for the higher-than-expected dust fluxes beyond 40 au include: radiation pressure extending the grain distribution beyond their source objects, the prescense of icy grains with different dynamical behavior than silicate grains, and the expectation of more dust-producing objects than previous models allowed for (Doner et al., 2024).

While radiation pressure initially extends the distribution of small grains beyond their source objects, equilibrium distribution is governed by long-term processes, such as Poynting-Robertson (PR) drag (Wyatt and Whipple, 1950; Burns, Lamy, and Soter, 1979). Radiation

pressure alone cannot explain the observed higher number densities reported by SDC, as it would not cause the originally predicted dust density peak to shift outward beyond 40 au (Doner et al., 2024).

Here, we focus on the possibility of a population of grains with different dynamical behavior than silicate grains. Kuiper Belt Objects (KBOs) have surfaces that are a mixture of rocky, carbonaceous, and icy material (Brown, 2012; Brown and Fraser, 2023) which, in response to mutual collisions and bombardment, produce rock grains, carbonaceous grains, ice grains, or mixed composition grains. While previous models assumed only silicate grains, here we consider the test case in which both pure silicate and pure ice grains are produced to gauge the difference in their dynamical behavior. Ice grains undergo rapid destruction by ultraviolet (UV) photo-sputtering and therefore exhibit different dynamical behavior than silicate grains (Grigorieva et al., 2007). We also consider that the KB may extend much beyond our current estimates (Fraser et al., 2024), as this could also have an effect on the equilibrium dust distribution.

2 The Student Dust Counter

SDC is composed of 14 Polyvinylidene Fluoride (PVDF) sensors. 12 of the sensors are oriented in the ram direction of the spacecraft and the remaining 2 are on the back side of the instrument, shielded from any dust and acting as controls (M. Horányi et al., 2008). The instrument has a total operating area of $\sim$0.1 m^2. The individual PVDF sensors are permanently electrically polarized and undergo a change in surface charge density when a hyper-velocity dust impact penetrates the conductive surface coating (M. Horányi et al., 2008). The measured impact-generated charge is a function of the impactor's mass and velocity. The number of electrons generated in an event is shown in Equation 1 (M. Horányi et al., 2008; James, Hoxie, and Horanyi, 2010; M. Piquette, James, and M. Horányi, 2020):

$$N_e = 3.8 * 10^{17} \times m^{1.3} v^{3.0}. \quad (1)$$

Grain mass, m, can be calculated from the measured charge, N_e, and the assumption that the spacecraft velocity dominates the impact velocity, v, which is ∼13 km/s recently. This assumption is valid for grains with generally circular Keplerian orbits and relatively slow orbital speeds, but does not hold true for the much smaller, but faster interstellar dust (ISD) grains. New Horizons has a heading of ∼293° along the ecliptic longitude compared to the ∼259° ISD inflow. Thus, ISD grains impact SDC at an angle of ∼23° off normal at a relative speed of ∼39 km/s (Bernardoni et al., 2022). The New Horizons flight path and ISD inflow can be seen in the left-hand side of Figure 1.

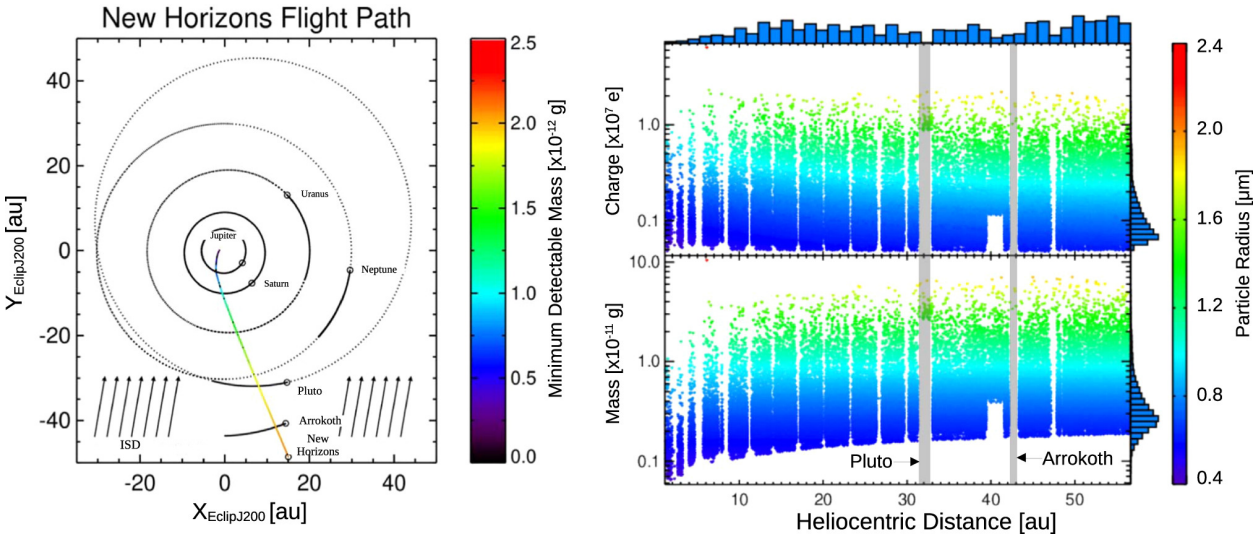

Figure 1: **Left:** New Horizons flight path through 55 au in the J2000 reference frame. SDC minimum detectable mass is indicated by the color scale and increasing as New Horizons is slowing down due to the gravity of the Sun. The giant planets Jupiter, Saturn, Uranus, and Neptune, along with KBOs Pluto and Arrokoth, and the ISD inflow are shown. **Right:** All non-coincident SDC data above the minimum mass threshold as both measured impact charge and calculated grain mass with the corresponding radius indicated by the color scale through July 25th, 2023. The shaded regions indicate periods of high spacecraft activity during close encounters with Pluto and Arrokoth. Figure adapted from Doner et al., 2024.

The higher impact velocities for ISDs make it such that their mass, which is calculated from the assumed impact velocity, is misinterpreted as a greater mass. Therefore, despite

having grain sizes below SDC mass thresholds, ISD impacts can be misinterpreted as larger particles and contribute to the density measurement as such (Bernardoni et al., 2022). The expected contribution of ISD grains to SDC has been modeled and is ∼5 times lower than Kuiper Belt dust out until ∼40 au. The instrument's electronics have been stable (i.e. reporting the correct mass for an impact) since launch in 2006 (Fountain et al., 2023), and its observations have been periodically reported in the literature (A. Poppe et al., 2010; Han et al., 2011; Szalay, Marcus Piquette, and Mihály Horányi, 2013; Bagenal et al., 2016; M. Piquette, A. R. Poppe, et al., 2019; Bernardoni et al., 2022; Doner et al., 2024). SDC observations can be seen in the right-hand side of Figure 1 and the corresponding number density measurements in Figure 2.

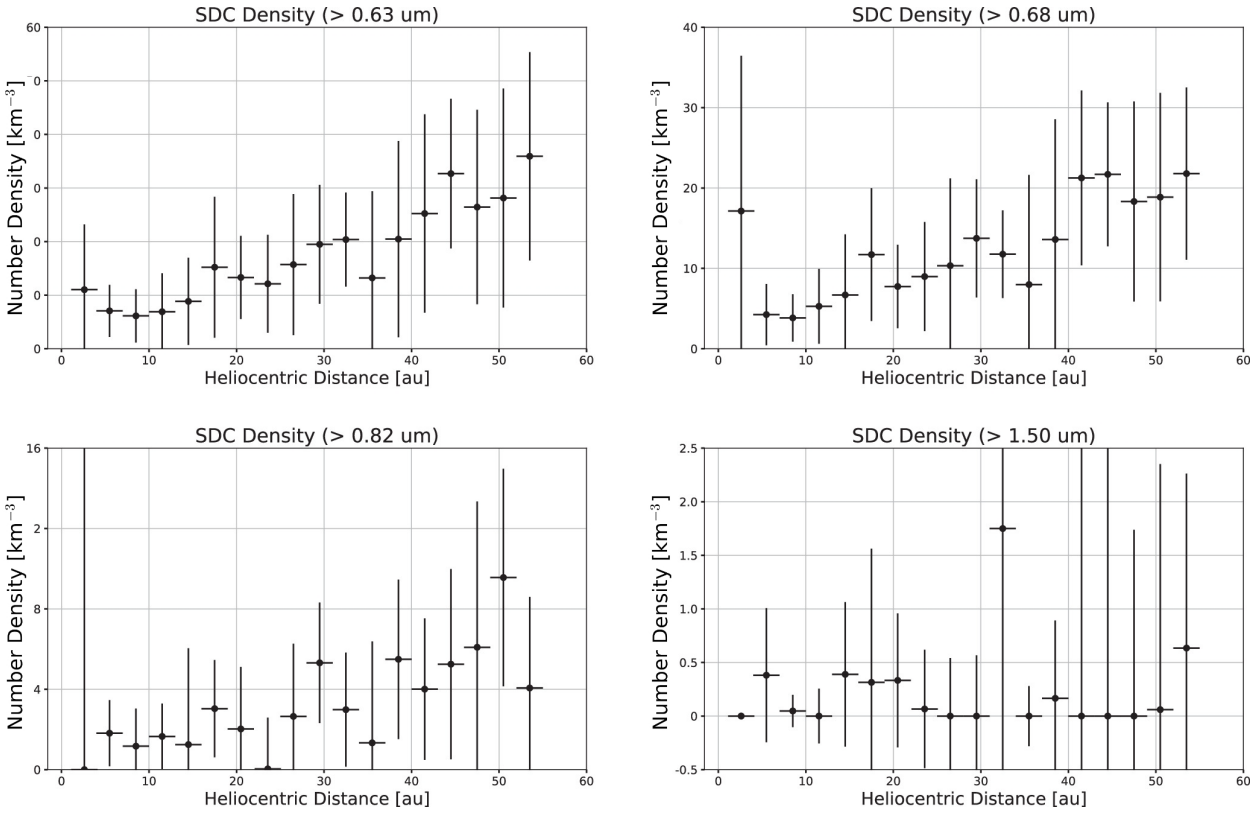

Figure 2: SDC density measurements above 4 cutoff sizes: 0.63 μm, 0.68 μm, 0.82 μm, and 1.50 μm. The 0.63 μm, 0.82 μm, and 1.50 μm cutoff sizes are chosen based on instrument thresholds, whereas the 0.68 μm cutoff size is chosen to avoid any contribution from ISDs. Figure adapted from Doner et al., 2024.

3 Source Objects

Jupiter-family comets, Halley-type comets, the asteroid belt, and the Trojan asteroids are the dominant source of dust in the inner Solar System, while the KB is the dominant source of dust in the outer Solar System (Landgraf et al., 2002; Andrew R. Poppe, 2016). Oort cloud comets contribute to the dust density only around 5-10 au, otherwise negligible (Andrew R. Poppe, 2016). KB dust production mainly results from mutual collisions (Stern, 1996) and interstellar dust bombardment (Yamamoto and Mukai, 1998) at similar rates.

We use various KBO databases/models to investigate the effects of an extended KB. The least extended list of KBOs is NASA/JPL's Small Bodies Database (SBDB), a database of objects with orbital elements determined by direct observation. The Canada-France Ecliptic Plane Survey (CFEPS), which applies a survey simulator to correct for observational biases, includes more distant objects with higher eccentricities and inclinations as well as densely populated mean-motion resonances (MMR) with Neptune (Kavelaars et al., 2009; B. Gladman and CFEPS Team, 2010; Petit et al., 2011). The Outer Solar System Origins Survey (OSSOS) is the most recent and comprehensive de-biased KBO model, containing over 26 million modeled objects (Bannister, Kavelaars, et al., 2016; Bannister, B. J. Gladman, et al., 2018; Lawler et al., 2018). Figure 3 shows the orbital distribution of each KBO database/model.

The Kuiper Belt can be grouped into 4 main populations: classical, resonant, scattered disk, and detached. Classical KBOs are the largest population and have stable orbits concentrated between ∼42–47 au (Malhotra, 2019). Resonant KBOs are trapped in mean motion resonances with Neptune (i.e. their orbital periods are in integer ratios with Neptune's). Scattered disk KBOs have highly eccentric orbits with perihelia between 30–38 au and semi-major axes extending beyond 1000 au (Malhotra, 2019). Detached KBOs are similar to scattered disk KBOs but have perihelia above ∼40 au, and are not influenced strongly by Neptune (Malhotra, 2019). To better compare the different databases/models, Figure 4

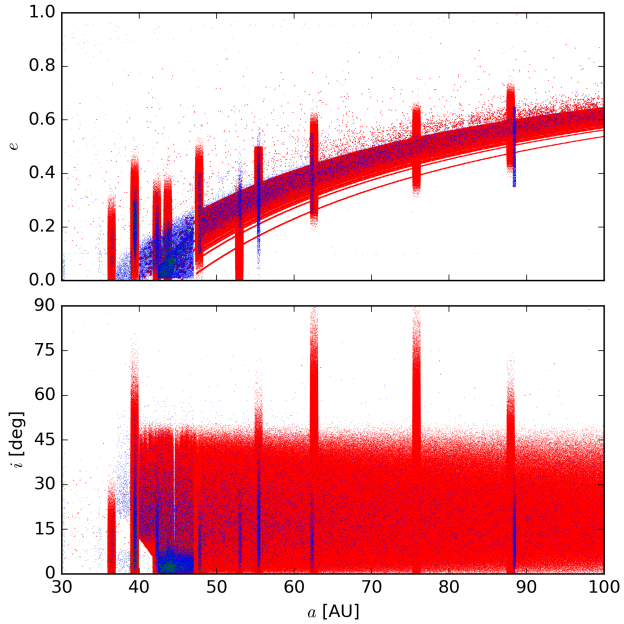

Figure 3: KBO orbital elements for the SBDB (green), CFEPS (blue), and OSSOS (red) databases/models. **Top:** eccentricity, e, as a function of semi-major axis, a. **Bottom:** inclination i as a function of semi-major axis, a.

shows the orbital distribution of each KBO database/model, normalized to an area of 1 for comparison.

The SBDB, as seen in Figure 4, has a large population of classical KBOs with semi-major axes between ∼42–47 au and low eccentricities and inclinations. The CFEPS and OSSOS models have fewer classical KBOs relative to other populations, as the number of resonant, scattered disk, and detached KBOs is much higher in these de-biased models.

4 Grain Dynamics

Newly released grains initially share the dynamical state vector of their source object. However, due to their small size, grains experience perturbations from solar radiation, which influences their subsequent trajectories. For a perfectly absorbing grain, these forces can be decomposed into two main components: radiation pressure and Poynting-Robertson drag. Radiation pressure is an outwardly radial force that arises due to the initial interception by

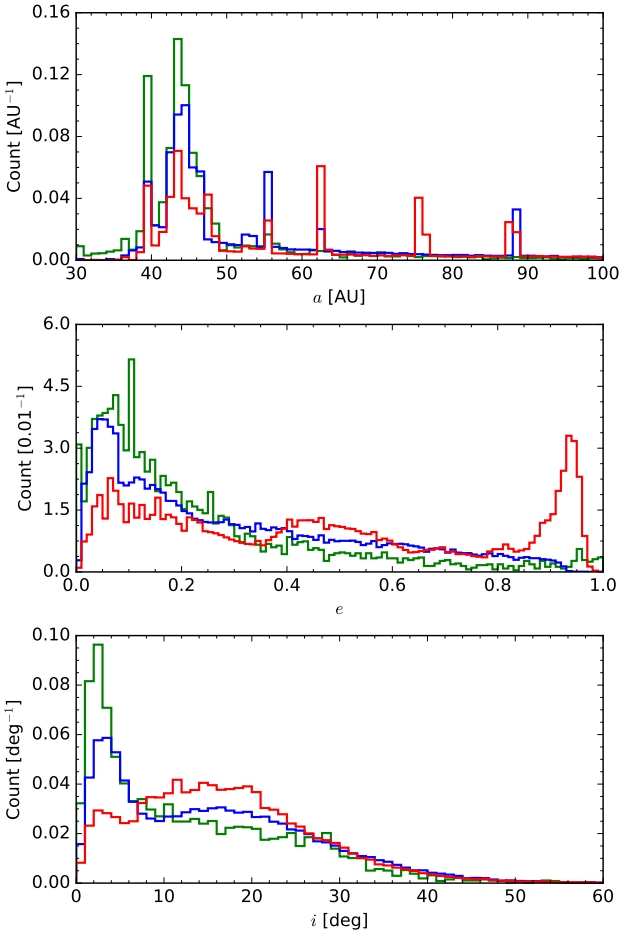

Figure 4: Normalized distributions of KBO orbital elements. From top to bottom: the semi-major axis, eccentricity, and inclination of the SBDB (green), CFEPS (blue), and OSSOS (red) distributions.

the grain of the momentum carried by the incident radiation. Poynting-Robertson drag is a mass loading drag that arises due to the re-radiation of the absorbed incident radiation by the grain with velocity $\mathbf{v}$. In the rest frame of the grain, the re-radiation is essentially isotropic, but in the inertial frame of the Sun, has some momentum in the $\hat{\mathbf{v}}$ direction.

Radiation pressure induces an instantaneous potential change, effectively reducing the solar mass by a factor of $1 - \beta$, where β is defined as F_r/F_g, the ratio of the radiation pressure force over gravity from the Sun. The parameter β is a function of the size, density, and optical properties of the grain and remains independent of the heliocentric distance (Burns, Lamy, and Soter, 1979). Figure 5 shows the β parameter for silicate and ice grains

as a function of grain radius.

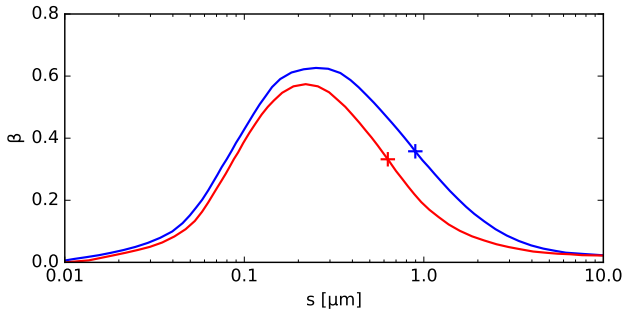

Figure 5: Radiation pressure parameter β for silicate (red) and ice (blue) grains as a function of grain radius s (Burns, Lamy, and Soter, 1979). SDC mass thresholds for both silicate and ice grains are shown as crosses with the respective color.

The subsequent orbital evolution of the grain is governed by PR drag, causing the grain to lose energy and angular momentum over longer time scales (Wyatt and Whipple, 1950). Gravitational interactions with the giant planets also influence grain dynamics (Liou, Zook, and Jackson, 1999; Moro-Martín et al., 2008). Without planetary perturbations, a simplified grain trajectory is given by the equation of motion

$$\ddot{\mathbf{r}} \approx \frac{\mu}{r^2}[(\beta - 1)\hat{\mathbf{r}} - \beta\frac{\mathbf{v}}{c}], \tag{2}$$

where $\mathbf{r}$ is the heliocentric position, μ is the standard gravitational parameter of the Sun equal to $GM_\odot$, with the gravitational constant G and solar mass $M_\odot$, $\mathbf{v}$ is the velocity vector of the grain, and c is the speed of light. The $\hat{\mathbf{r}}$ term includes both gravity from the Sun and radiation pressure, while the $\mathbf{v}$ term is the PR drag.

The fastest erosion process for silicate grains is solar-wind-induced sputtering, with a rate of $\sim$0.2 Å yr^{-1} at 1 au (Mukai et al., 2001). Ice undergoes much more rapid erosion due to UV photo-sputtering, with a rate of $\sim$40 Å yr^{-1} at 1 au (Harrison and Schoen, 1967; Carlson, 1980). Both rates decrease with heliocentric distance as $1/r^2$. Ice also experiences sublimation, but this process is much slower in the outer Solar System than UV photo-sputtering due to the low local equilibrium temperatures (Patashnick and Rupprecht, 1977;

Lisse, Young, et al., 2021), and thus not included in this model.

Grains with slow erosion rates, like silicate grains, migrate inward due to PR drag, whereas grains with rapid erosion rates, like ice, initially migrate outward as the continually increasing radiation pressure can overcome PR drag (Grigorieva et al., 2007). As the grain continues to erode, its radiation pressure coefficient reaches a maximum and begins to decrease (Burns, Lamy, and Soter, 1979). Eventually, the grain begins to migrate inward. This inward migration due to decreasing radiation pressure occurs only for grains below the SDC mass threshold. Figure 6 shows the orbital evolution of example silicate and ice grains, with identical initial conditions.

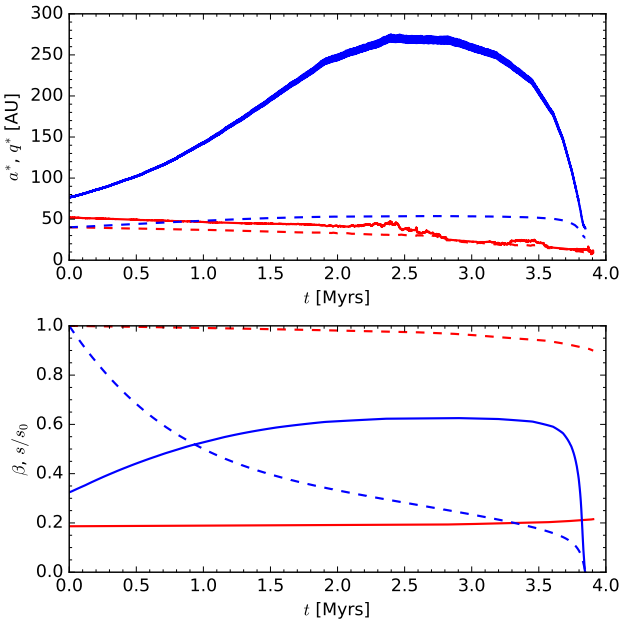

Figure 6: Numerically integrated orbital evolution of initially 1 μm radius silicate (red) and ice (blue) grains from a source object on a circular orbit at 40 au, inclined by 5°. **Top:** Evolution of the semi-major axis (solid) and perihelion distance (dashed). These orbital elements are calculated with $\mu^* = \mu(1 - \beta)$ and represent the grain's orbital geometry. **Bottom:** Evolution of radiation pressure parameter (solid) and the ratio of grain size to initial grain size (dashed).

5 Dust Production

Dust production in the KB is approximated by ejecting a grain at a random time within the orbit of a randomly selected KBO. This approximation is consistent with ejection via interstellar dust bombardment or other mechanisms independent of heliocentric distance (Belousov and Pavlov, 2024), but not with mutual collisions since those will preferentially occur closer to perihelion, where the objects have higher orbital speeds and spatial densities. We choose to use this approximation because it possible to numerically solve, while modeling mutual collisions would be very difficult. Dust production due to mutual collision depends on collisional probabilities, velocities, cross sections, etc.

The semi-major axis, eccentricity, and inclination of the KBO are obtained from the respective KBO database/model, and the orbital orientation is determined by assigning random values to the longitude of the ascending node ($0 \leq \Omega \leq 2\pi$) and the argument of periapsis ($0 \leq \omega \leq 2\pi$). The ejection position and velocity are calculated by solving Kepler's equation $M = E - e\sin(E)$ (Danby, 1992) to determine the eccentric anomaly, E, using a randomly selected mean anomaly ($0 \leq M \leq 2\pi$). Figure 7 shows examples of solutions to Kepler's equation. The choices of these orbital elements fully determine the initial position $\mathbf{r}$ and velocity $\mathbf{v}$ of a released grain.

Figure 8 shows how the initial grain radius, s, is randomly sampled following a power-law distribution, $n(s) \propto s^{-\alpha}$, with $\alpha = 3.5$, consistent with a collisional equilibrium and observed dust disks (Dohnanyi, 1969; Ricci et al., 2015; MacGregor et al., 2016).

Densities of 2.7 g/cm^3 and 0.92 g/cm^3 are assumed for silicate and ice grains, respectively, as expected for submicron grains in KBOs (Lisse, A'Hearn, et al., 1998). The evolution of the size, hence β, due to UV photo-sputtering or solar-wind induced sputtering is followed by simultaneously integrating it with Equation 2.

Equation 2, with the addition of gravitational forces from Jupiter, Saturn, Uranus, and Neptune, is integrated using a fourth/fifth order adaptive stepsize Runge–Kutta–Fehlberg

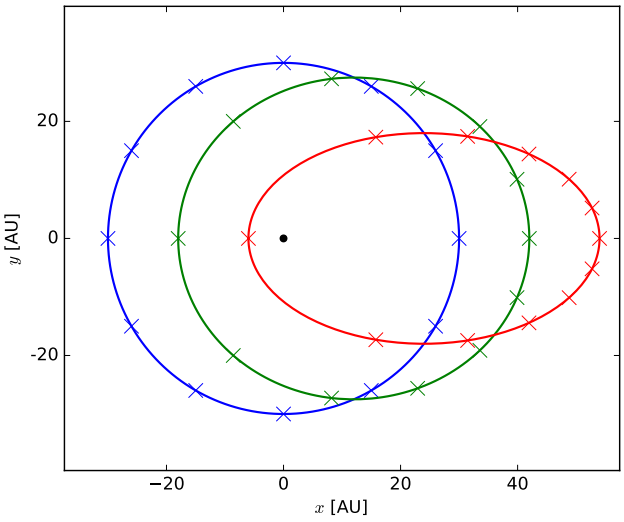

Figure 7: Keplerian orbits for example objects with semi-major axes $a = 30$ au and eccentricities $e = 0.0$ (blue), $e = 0.4$ (green), and $e = 0.8$ (red). The crosses indicate the positions of the objects at evenly spaced time intervals, determined by solving Kepler's equation for uniformly distributed mean anomalies.

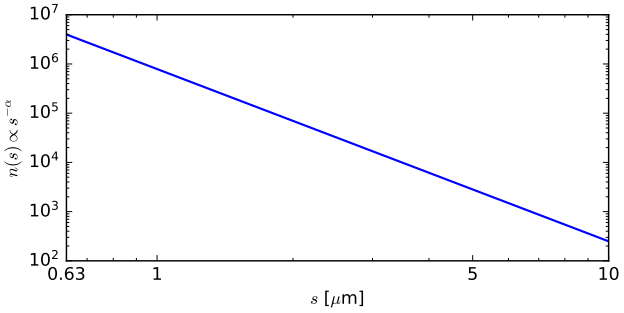

Figure 8: Normalized probability density $n(s)$ as a function of initial grain radius s.

method (Fehlberg, 1969; Press et al., 2002), which accurately resolves close encounters with the planets. All KBOs are included in the model as potential source objects. To achieve similar statistics for both populations, a total of 10,000 silicate grains and 500,000 ice grains were simulated for each KBO database/model. Grains are only removed from the simulation when their orbital energy becomes greater than zero, indicating an unbound orbit, or their mass falls below the SDC detection threshold. A slice of the 3D equilibrium density distribution, extending ±0.5 au above and below the ecliptic plane, is used to compare directly with SDC measurement.

One thing to consider is that ice grains have lower densities and tensile strength than

silicate grains, resulting in a lower cratering efficiency. An ice particle with the same mass as a silicate particle would likely have a weaker PVDF signal as a result. This introduces some error into the model and should be studied further.

6 Results

Figure 9 shows the equilibrium number density profiles of silicate and ice grains near the ecliptic, fitted to SDC data using χ^2 minimization, varying only the silicate and ice production rates (i.e. adjust the mass production rates, scaling the histograms vertically until χ^2 is at a minimum, indicating best fit), keeping all other simulation variables constant (Press et al., 2002). Contrary to expectations, the de-biased KBO models CFEPS and OSSOS, which include many more distant objects, do not exhibit a more distant silicate number density peak as compared to the observational SBDB database. Instead, silicate number densities between 40 and 60 au are slightly lower in the de-biased models because dust from the distant, high-inclination KBOs do not contribute to the equilibrium number density profile near the ecliptic as much as closer, low-inclination KBOs would. Despite these variations in the silicate equilibrium distribution, the silicate mass production rate remains generally consistent across all KBO models.

The ice number density peak is more distant than the silicate peak. Most ice grains initially migrate outward due to radiation pressure and erosion and have a negligible contribution within Neptune's orbit. Due to their shorter lifetimes and greater heliocentric distances, ice grains have lower number densities than silicate grains at the same production rates, necessitating a higher ice production rate to fit SDC data. This finding is consistent with the ice content of KBOs (Brown, 2012; Brown and Fraser, 2023) and laboratory impact crater experiments which show that the ejected mass yield increases by over an order of magnitude going from a pure silicate to a pure ice surface (Lange and Ahrens, 1987; Koschny and Grün, 2001). This tendency of enhanced yield with increasing ice content was

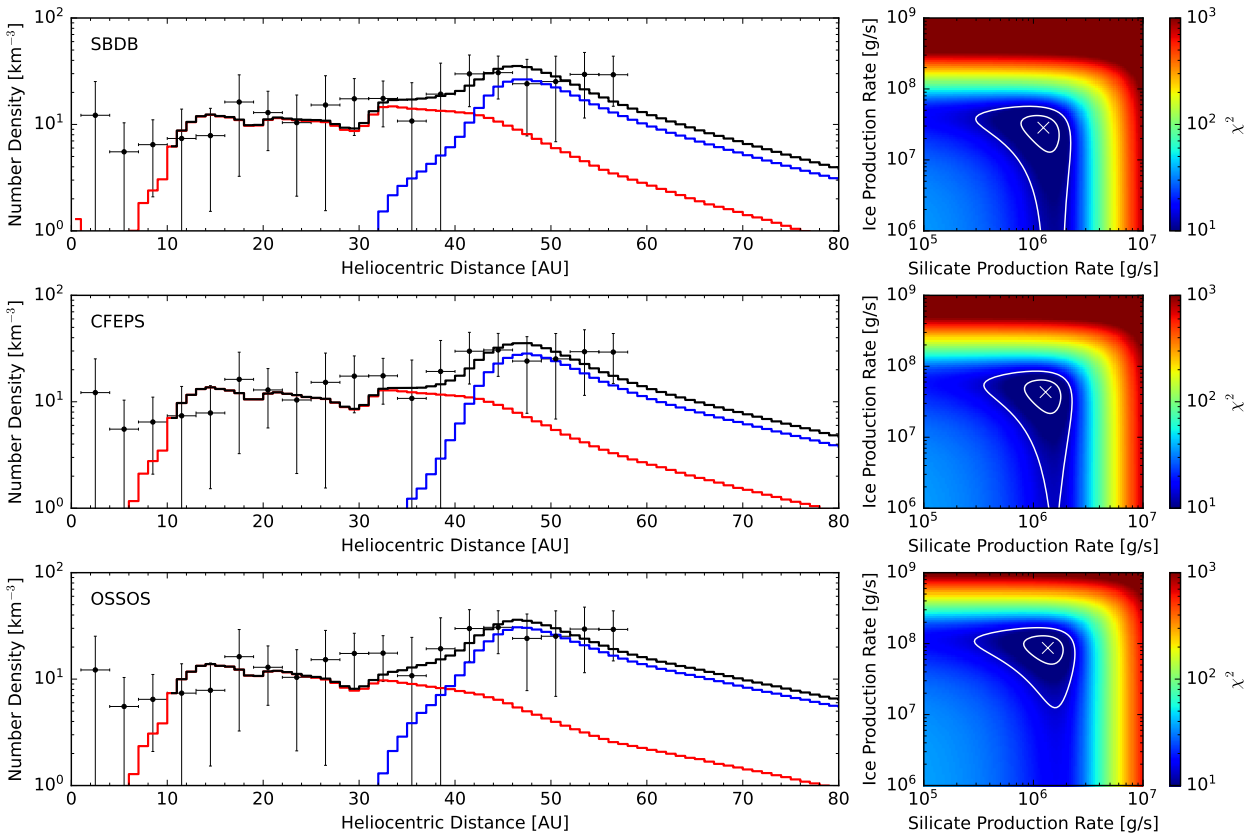

Figure 9: **Left:** Equilibrium number density profiles of silicate and ice grains near the ecliptic and above the SDC mass threshold as a function of heliocentric distance using the SBDB (top), CFEPS (middle) and OSSOS (bottom) KBO databases/models. The combined modeled number density (black) of silicate (red) and ice (blue) grains is fitted to SDC data with 1σ error bars (black) for heliocentric distances greater than 10 au. **Right:** Corresponding χ^2 maps of silicate and ice mass production rates for each KBO database/model with best-fit production rates (white crosses). Regions of confidence corresponding to a significance level of $\alpha = 0.68$ and $\alpha = 0.99$, or 1σ and 3σ, respectively, are encircled in white lines. 1σ production rate ranges can be found in Table 1.

also observed by the *Galileo* mission in the dust exospheres engulfing the large icy moons of Jupiter (Krivov et al., 2003).

Table 1 lists our estimates for silicate and ice production rates in the KB. Previous estimates of the KB silicate mass production rate matching early SDC data were in the range of 8.4×10^5 to 9.4×10^5 g/s (Han et al., 2011) and 6×10^6 to 1×10^7 (A. R. Poppe et al., 2019). These models were constrained by available SDC data out to only 20 au and 40 au, respectively. Consequently, these production rates were not informed by the measured

dust densities beyond 40 au.

KBO database/model	Silicate production rate [g/s]	Ice production rate [g/s]	Ice to silicate production ratio
SBDB	7.7×10^5 to 1.7×10^6	1.3×10^7 to 4.2×10^7	∼20
CFEPS	8.3×10^5 to 1.8×10^6	2.2×10^7 to 6.4×10^7	∼30
OSSOS	8.1×10^5 to 1.9×10^6	5.1×10^7 to 1.3×10^8	∼70

Table 1: Mass production rates of 0.1 to 10 μm silicate and ice grains for various KBO databases/models fitted to SDC data in the 1σ significance level.

Theoretical estimates for the mass production rate in the KB are 8.6×10^4 to 2.9×10^7 g/s from mutual collisions (Stern, 1996) and 3.7×10^5 to 3.1×10^7 g/s from interstellar dust bombardment (Yamamoto and Mukai, 1998). Our model results are consistent with the upper ranges of these estimates. The wide range of theoretical estimates should be revisited based on our more complete recent understanding of the KB (Malhotra, 2019), and the interstellar dust flux (Krüger and Grün, 2009).

7 Discussion

The model discussed so far focused on pure silicate and water-ice grains. In reality, grains are likely composed of a mixture of rocky, carbonaceous, and volatile matter (Burns, Lamy, and Soter, 1979; Grigorieva et al., 2007; Brown and Fraser, 2023), with dynamical evolution that might not be bracketed by the assumed single composition grains modeled here.

Thus, we briefly explore two scenarios of refractory/volatile mixtures: well-mixed and differentiated grains. For well-mixed grains, we approximate the radiation pressure coefficient as a surface-fraction-weighted average. Since weakly bound grains also lose rocky material with eroding ice, we keep the ice mass fraction fixed and approximate the erosion rate also as a surface-fraction-weighted average. This simplification keeps the volatile-refractory ratio constant and avoids the complexity of developing differentiated layers within a dust grain. For differentiated grains with a rocky core and ice mantle, we use the radiation pressure coefficient and erosion rate for pure ice until the mantle erodes, at which point we switch to those of pure silicate. Figure 10 shows the equilibrium distributions of grains for both cases.

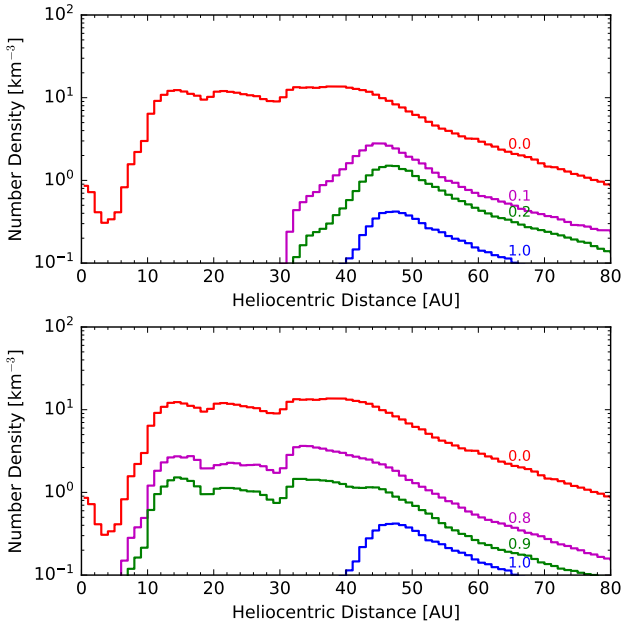

Figure 10: Equilibrium number density profiles of well-mixed (top) and differentiated (bottom) grains near the ecliptic and above the SDC mass threshold as a function of heliocentric distance using the SBDB KBO database. Each histogram is labeled with its corresponding ice mass fraction. The same number of grains is produced for each case, matching the best-fit silicate production rate for the SBDB KBO database in Table 1.

The equilibrium distribution for well-mixed grains resembles that of pure ice but with higher number densities due to the slower erosion and therefore longer lifetimes. For differentiated grains, the equilibrium distribution resembles that of pure silicate but with lower number densities because the ice mantle rapidly erodes and the grain eventually behaves like pure silicate, but grains can drop below the SDC mass threshold in this process. The preliminary results indicate that even a low ice content can have a large impact on equilibrium distributions, suggesting that the ice production rate may not need to be as high to fit SDC data. These rough models are intended simply to motivate future research that captures more realistic grain compositions and behaviors.

8 Conclusion

We have estimated the equilibrium distributions and mass production rates of silicate and ice grains in the outer Solar System using various KBO databases/models as source objects. This work suggests that the equilibrium dust distributions are relatively independent of the three source object distributions we used and are more dependent on the assumed composition of the grains. Hence, without measuring grain composition, SDC measurements to date do not fully constrain the extent of the KB.

For the case in which pure silicate and pure ice grains are produced, we estimate that the mass production rate of 0.1 to 10 μm ice grains is 20 to 70 times higher than for silicate grains, consistent with the ice content of KBOs (Brown, 2012; Brown and Fraser, 2023) and the high yield from impacts on these surfaces (Lange and Ahrens, 1987; Koschny and Grün, 2001; Krivov et al., 2003). These estimates should be refined for the more realistic cases of mixed-composition grains.

Significant deviation from the predicted decline of dust densities in future SDC measurements would prompt us to revisit the assumptions used in this paper. A continued increase in measured dust densities may suggest an undiscovered, unexpectedly massive population of distant source objects, while a more rapid decrease in measured dust densities may suggest refractory dominant or differentiated grain compositions that, dynamically, look like silicate grains.

The suggestion of distant icy grains has implications for our understanding of dust disks and may impact the interpretation of observed extrasolar dust disks, as similar processes are expected to occur in other Solar Systems (Pontoppidan et al., 2005; Terada et al., 2007; Chen, Fitzgerald, and Smith, 2008; Honda et al., 2009). Advances in detecting both the spatial distributions and compositions of extrasolar dust disks will enhance our understanding of these processes (Hughes, Duchêne, and Matthews, 2018; Kim, Kennedy, and Roccatagliata, 2024). The distinct dynamics of the inwardly-migrating refractory and the outwardly-

migrating volatile grains result in composition-differentiated spatial distributions that, when resolved, may help constrain the spatial distribution of the corresponding extrasolar source objects.

Continued SDC measurements at greater heliocentric distances will further constrain our models of the production, transport, and destruction of dust in the outer Solar System.

References

Bagenal, F. et al. (Mar. 2016). "Pluto' interaction with its space environment: Solar wind, energetic particles, and dust". In: *Science* 351.6279, aad9045, aad9045. DOI: 10.1126/science.aad9045. arXiv: 1605.00749 [astro-ph.EP].

Bannister, Michele T., Brett J. Gladman, et al. (May 2018). "OSSOS. VII. 800+ Trans-Neptunian Objects—The Complete Data Release". In: *The Astrophysical Journals* 236.1, 18, p. 18. DOI: 10.3847/1538-4365/aab77a. arXiv: 1805.11740 [astro-ph.EP].

Bannister, Michele T., J. J. Kavelaars, et al. (Sept. 2016). "The Outer Solar System Origins Survey. I. Design and First-quarter Discoveries". In: *The Astronomical Journal* 152.3, 70, p. 70. DOI: 10.3847/0004-6256/152/3/70. arXiv: 1511.02895 [astro-ph.EP].

Belousov, D. V. et al. (June 2024). "Cometary outbursts in the Oort cloud". In: *Icarus* 415, 116066, p. 116066. DOI: 10.1016/j.icarus.2024.116066. arXiv: 2312.14314 [astro-ph.EP].

Bernardoni, Edwin et al. (Mar. 2022). "Student Dust Counter Status Report: The First 50 au". In: *The Planetary Science Journal* 3.3, 69, p. 69. DOI: 10.3847/PSJ/ac5ab7.

Brown, Michael E. (May 2012). "The Compositions of Kuiper Belt Objects". In: *Annual Review of Earth and Planetary Sciences* 40.1, pp. 467–494. DOI: 10.1146/annurev-earth-042711-105352. arXiv: 1112.2764 [astro-ph.EP].

Brown, Michael E. et al. (July 2023). "The State of CO and CO_2 Ices in the Kuiper Belt as Seen by JWST". In: *The Planetary Science Journal* 4.7, 130, p. 130. DOI: 10.3847/PSJ/ace2ba. arXiv: 2306.17051 [astro-ph.EP].

Burns, J. A. et al. (Oct. 1979). "Radiation forces on small particles in the solar system". In: *Icarus* 40, pp. 1–48. DOI: 10.1016/0019-1035(79)90050-2.

Carlson, R. W. (Jan. 1980). "Photo-sputtering of ice and hydrogen around Saturn's rings". In: *Nature* 283.5746, p. 461. DOI: 10.1038/283461a0.

Chen, Christine H. et al. (Dec. 2008). "A Possible Icy Kuiper Belt around HD 181327". In: *The Astrophysical Journal* 689.1, pp. 539–544. DOI: 10.1086/592567. arXiv: 0808.2273 [astro-ph].

Christon, S. P. et al. (2015). "Discovery of suprathermal Fe+ in Saturn's magnetosphere". In: *Journal of Geophysical Research: Space Physics* 120.4, pp. 2720–2738. DOI: https://doi.org/10.1002/2014JA020906. eprint: https://agupubs.onlinelibrary.wiley.com/doi/pdf/10.1002/2014JA020906. URL: https://agupubs.onlinelibrary.wiley.com/doi/abs/10.1002/2014JA020906.

Danby, John M. A. (1992). *Fundamentals of celestial mechanics*.

Dohnanyi, J. S. (May 1969). "Collisional Model of Asteroids and Their Debris". In: *Journal of Geophysical Research* 74, pp. 2531–2554. DOI: 10.1029/JB074i010p02531.

Doner, Alex et al. (Feb. 2024). "New Horizons Venetia Burney Student Dust Counter Observes Higher than Expected Fluxes Approaching 60 au". In: *The Astrophysical Journal Letters* 961.2, L38, p. L38. DOI: 10.3847/2041-8213/ad18b0. arXiv: 2401.01230 [astro-ph.EP].

Fehlberg, E. (1969). *Low-order classical Runge-Kutta formulas with stepsize control and their application to some heat transfer problems*. Technical Report NASA-TR-R-315.

Fountain, G.H. et al. (2023). *The New Horizons Instrument Suite*. Technical Digest 37-1. Johns Hopkins APL.

Fraser, Wesley C. et al. (Oct. 2024). "Candidate Distant Trans-Neptunian Objects Detected by the New Horizons Subaru TNO Survey". In: *The Planetary Science Journal* 5.10, 227, p. 227. DOI: 10.3847/PSJ/ad6f9e. arXiv: 2407.21142 [astro-ph.EP].

Gladman, Brett et al. (Oct. 2010). "The Canada France Ecliptic Plane Survey: CFEPS-L7 Data Release". In: *AAS/Division for Planetary Sciences Meeting Abstracts #42*. Vol. 42. AAS/Division for Planetary Sciences Meeting Abstracts, 40.11, p. 40.11.

Grigorieva, A. et al. (Nov. 2007). "Survival of icy grains in debris discs. The role of photosputtering". In: *Astronomy & Astrophysics* 475.2, pp. 755–764. DOI: 10.1051/0004-6361:20077686. arXiv: 0709.0811 [astro-ph].

Han, D. et al. (Dec. 2011). "Constraints on dust production in the Edgeworth-Kuiper Belt from Pioneer 10 and New Horizons measurements". In: *Geophys. Res. Lett.* 38, L24102, p. 24102. DOI: 10.1029/2011GL050136.

Harrison, Halstead et al. (Sept. 1967). "Evaporation of Ice in Space: Saturn's Rings". In: *Science* 157.3793, pp. 1175–1176. DOI: 10.1126/science.157.3793.1175.

Hillier, J. K. et al. (June 2007). "The composition of Saturn's E ring". In: 377, pp. 1588–1596. DOI: 10.1111/j.1365-2966.2007.11710.x.

Honda, M. et al. (Jan. 2009). "Detection of Water Ice Grains on the Surface of the Circumstellar Disk Around HD 142527". In: *The Astrophysical Journal Letters* 690.2, pp. L110–L113. DOI: 10.1088/0004-637X/690/2/L110.

Horányi, M. et al. (Oct. 2008). "The Student Dust Counter on the New Horizons Mission". In: *Space Sci. Rev.* 140, pp. 387–402. DOI: 10.1007/s11214-007-9250-y.

Hughes, A. Meredith et al. (Sept. 2018). "Debris Disks: Structure, Composition, and Variability". In: *Annual Review of Astronomy and Astrophysics* 56, pp. 541–591. DOI: 10.1146/annurev-astro-081817-052035. arXiv: 1802.04313 [astro-ph.EP].

James, D. et al. (Mar. 2010). "Polyvinylidene fluoride dust detector response to particle impacts". In: *Review of Scientific Instruments* 81.3, 034501-034501-8, pp. 034501-034501–8. DOI: 10.1063/1.3340880.

Kavelaars, J. J. et al. (June 2009). "The Canada-France Ecliptic Plane Survey—L3 Data Release: The Orbital Structure of the Kuiper Belt". In: *The Astronomical Journal* 137.6, pp. 4917–4935. DOI: 10.1088/0004-6256/137/6/4917.

Kim, Minjae et al. (Aug. 2024). "The characterization of water ice in debris discs: implications for JWST scattered light observations". In: *Monthly Notices of the Royal Astronomical Society* 533.3, pp. 2801–2822. ISSN: 0035-8711. DOI: 10.1093/mnras/stae1923. eprint:

https://academic.oup.com/mnras/article-pdf/533/3/2801/58979597/stae1923.pdf. URL: https://doi.org/10.1093/mnras/stae1923.

Koschny, D. et al. (Dec. 2001). "Impacts into Ice-Silicate Mixtures: Crater Morphologies, Volumes, Depth-to-Diameter Ratios, and Yield". In: *Icarus* 154, pp. 391–401. DOI: 10.1006/icar.2001.6707.

Krivov, A. V. et al. (Mar. 2003). "Impact-generated dust clouds around planetary satellites: spherically symmetric case". In: *Planetary and Space Science* 51, pp. 251–269.

Krüger, H. et al. (Mar. 2009). "Interstellar Dust Inside and Outside the Heliosphere". In: *Space Science Reviews* 143, pp. 347–356. DOI: 10.1007/s11214-008-9431-3. arXiv: 0802.3787.

Landgraf, M. et al. (May 2002). "Origins of Solar System Dust beyond Jupiter". In: *The Astronomical Journal* 123, pp. 2857–2861. DOI: 10.1086/339704. eprint: arXiv:astro-ph/0201291.

Lange, M. A. et al. (Mar. 1987). "Impact experiments in low-temperature ice". In: *Icarus* 69.3, pp. 506–518. DOI: 10.1016/0019-1035(87)90020-0.

Lawler, Samantha M. et al. (May 2018). "OSSOS: X. How to use a Survey Simulator: Statistical Testing of Dynamical Models Against the Real Kuiper Belt". In: *Frontiers in Astronomy and Space Sciences* 5, 14, p. 14. DOI: 10.3389/fspas.2018.00014. arXiv: 1802.00460 [astro-ph.EP].

Liou, J.-C. et al. (Sept. 1999). "Orbital Evolution of Retrograde Interplanetary Dust Particles and Their Distribution in the Solar System". In: *Icarus* 141, pp. 13–28. DOI: 10.1006/icar.1999.6170.

Lisse, C. M., M. F. A'Hearn, et al. (Mar. 1998). "Infrared Observations of Comets by COBE". In: *The Astrophysical Journal* 496.2, pp. 971–991. DOI: 10.1086/305397.

Lisse, C. M., L. A. Young, et al. (Mar. 2021). "On the origin & thermal stability of Arrokoth's and Pluto's ices". In: *Icarus* 356, 114072, p. 114072. DOI: 10.1016/j.icarus.2020.114072. arXiv: 2009.02277 [astro-ph.EP].

MacGregor, Meredith A. et al. (Sept. 2016). "ALMA Observations of the Debris Disk of Solar Analog τ Ceti". In: *The Astrophysical Journal* 828.2, 113, p. 113. DOI: 10.3847/0004-637X/828/2/113. arXiv: 1607.02513 [astro-ph.SR].

Malhotra, Renu (Dec. 2019). "Resonant Kuiper belt objects: a review". In: *Geoscience Letters* 6.1, 12, p. 12. DOI: 10.1186/s40562-019-0142-2. arXiv: 1911.07897 [astro-ph.EP].

Moro-Martín, A. et al. (2008). "Extrasolar Kuiper Belt Dust Disks". In: *The Solar System Beyond Neptune*. Ed. by M. A. Barucci et al., pp. 465–480. DOI: 10.48550/arXiv.astro-ph/0703383.

Moses, Julianne I. (1992). "Meteoroid ablation in Neptune's atmosphere". In: *Icarus* 99.2, pp. 368–383. ISSN: 0019-1035. DOI: https://doi.org/10.1016/0019-1035(92)90153-X. URL: https://www.sciencedirect.com/science/article/pii/001910359290153X.

Mukai, T. et al. (2001). "Interplanetary Dust". In: ed. by E. Grün et al. Springer. Chap. Physical Processes on Interplanetary Dust, pp. 445–507.

Patashnick, H. et al. (Feb. 1977). "The Lifetime of Ice Particles in the Solar System". In: *Icarus* 30.2, pp. 402–412. DOI: 10.1016/0019-1035(77)90174-9.

Petit, J. -M. et al. (Oct. 2011). "The Canada-France Ecliptic Plane Survey—Full Data Release: The Orbital Structure of the Kuiper Belt". In: *The Astronomical Journal* 142.4, 131, p. 131. DOI: 10.1088/0004-6256/142/4/131. arXiv: 1108.4836 [astro-ph.EP].

Piquette, M., A. R. Poppe, et al. (Mar. 2019). "Student Dust Counter: Status report at 38 AU". In: *Icarus* 321, pp. 116–125. DOI: 10.1016/j.icarus.2018.11.012.

Piquette, M. et al. (Feb. 2020). "Calibration of polyvinylidene fluoride based dust detectors in response to varying grain density and incidence angle". In: *Review of Scientific Instruments* 91.2, 023307, p. 023307. DOI: 10.1063/1.5125448.

Pontoppidan, Klaus M. et al. (Mar. 2005). "Ices in the Edge-on Disk CRBR 2422.8-3423: Spitzer Spectroscopy and Monte Carlo Radiative Transfer Modeling". In: *The Astrophysical Journal* 622.1, pp. 463–481. DOI: 10.1086/427688. arXiv: astro-ph/0411367 [astro-ph].

Poppe, A. et al. (June 2010). "First results from the Venetia Burney Student Dust Counter on the New Horizons mission". In: *Geophys. Res. Lett.* 37, L11101, p. 11101. DOI: 10.1029/2010GL043300.

Poppe, A. R. et al. (Aug. 2019). "Constraining the Solar System's Debris Disk with In Situ New Horizons Measurements from the Edgeworth-Kuiper Belt". In: *The Astrophysical Journal Letters* 881.1, L12, p. L12. DOI: 10.3847/2041-8213/ab322a.

Poppe, Andrew R. (Jan. 2016). "An improved model for interplanetary dust fluxes in the outer Solar System". In: *Icarus* 264, pp. 369–386. DOI: 10.1016/j.icarus.2015.10.001.

Press, W. H. et al. (2002). *Numerical recipes in C++ : the art of scientific computing*. Cambridge University Press.

Ricci, L. et al. (Jan. 2015). "ALMA Observations of the Debris Disk around the Young Solar Analog HD 107146". In: *The Astrophysical Journal* 798.2, 124, p. 124. DOI: 10.1088/0004-637X/798/2/124. arXiv: 1410.8265 [astro-ph.EP].

Stern, S. A. (June 1996). "Signatures of collisions in the Kuiper Disk." In: *Astronomy & Astrophysics* 310, pp. 999–1010.

Szalay, Jamey R. et al. (Oct. 2013). "The Student Dust Counter: Status report at 23 AU". In: *Earth, Planets and Space* 65.10, pp. 1145–1149. DOI: 10.5047/eps.2013.02.005.

Terada, Hiroshi et al. (Sept. 2007). "Detection of Water Ice in Edge-on Protoplanetary Disks: HK Tauri B and HV Tauri C". In: *The Astrophysical Journal* 667.1, pp. 303–307. DOI: 10.1086/520951.

Thiessenhusen, K.-U. et al. (Jan. 2002). "A dust cloud around Pluto and Charon". In: *Planetary and Space Science* 50, pp. 79–87.

Wyatt, S. P. et al. (Jan. 1950). "The Poynting-Robertson effect on meteor orbits". In: *The Astrophysical Journal* 111, pp. 134–141. DOI: 10.1086/145244.

Yamamoto, S. et al. (Jan. 1998). "Dust production by impacts of interstellar dust on Edgeworth-Kuiper Belt objects". In: *Astronomy & Astrophysics* 329, pp. 785–791.